

Entropic Barriers and the Kinetic Suppression of Topological Defects

Yi-Lin Tsao¹ and Zhu-Xi Luo¹

¹*School of Physics, Georgia Institute of Technology, Atlanta, Georgia 30332, USA*

(Dated: February 20, 2026)

Many quantum phases, from topological orders to superfluids, are destabilized at finite temperature by the proliferation and motion of topological defects such as anyons or vortices. Conventional protection mechanisms rely on energetic gaps and fail once thermal fluctuations exceed the gap scale. Here we examine a complementary mechanism of entropic protection, in which defect nucleation is suppressed by coupling to mesoscopic auxiliary reservoirs of dimension M , generating an effective free-energy barrier that increases with temperature. In the Ising chain, this produces a characteristic three-regime evolution of the correlation length as a function of temperature — linear growth, entropy-controlled plateau, and eventual breakdown—indicating a general modification of defect behavior. Focusing on two spatial dimensions, where true finite-temperature topological order is forbidden in the thermodynamic limit, we show that entropic protection can nevertheless strongly enhance stabilization at finite system size, the regime directly relevant for quantum memory and experiments. Owing to the topological character of the defects, creation and transport are independently suppressed, yielding a double parametric reduction of logical errors in the entropic toric code and enhanced coherence when the framework is extended to Berezinskii–Kosterlitz–Thouless transitions. Entropic barriers thus provide a passive and scalable route to stabilizing quantum phases in experimentally relevant regimes. We propose an experimental setup for entropic toric code using dual species Rydberg arrays with dressing.

CONTENTS

I. Introduction	1
II. The Entropic Ising Chain	2
III. Entropic Protection of 2D Toric Code	3
A. Static stability	3
B. Dynamic Stability	4
C. Experimental setup	5
IV. Entropic Protection of Superfluids	5
V. Discussion and outlook	6
Acknowledgments	7
A. Modified Ising chain	7
B. Microscopic Derivation of Entropic Lindbladian	7
References	8

I. INTRODUCTION

Understanding how quantum phases persist or degrade at finite temperature is a central challenge in condensed matter physics and quantum information science. In two spatial dimensions, while topological order offers intrinsic protection against local perturbations [1], this protection is generically compromised by the proliferation of topological defects [2, 3]. In discrete gauge theories like the toric code, thermally activated point-like anyons diffuse and dephase logical memory [2–4]. Similarly, in

more conventional settings of two-dimensional superfluids, coherence is destroyed by the unbinding of vortex-antivortex pairs (BKT transition) [5]. The instability in both cases stems from the reliance on purely energetic protection: once the system’s extensive configurational entropy overcomes the static energetic tension of these defects, they proliferate and destroy global order.

Mitigating this fragility traditionally necessitates a trade-off between the substantial redundancy requirements of active quantum error correction [6–9] the geometric intractability of energetic self-correction via high-dimensional or fractal confinement [7, 10–12]. A promising alternative is autonomous quantum error correction, in which quantum information is stabilized through engineered dissipation without measurement-feedback loops [13, 14]. These protocols suppress errors by continuously removing entropy from the logical subspace [15], with the resulting protection being inherently dynamical and logical stability set by non-equilibrium rate balances rather than a thermodynamic free-energy barrier. In contrast, our approach fundamentally diverges by exploiting thermal entropy itself as a stabilizing resource, rather than continuously extracting it.

In this work, we examine a universal mechanism of entropic protection, where fluctuating auxiliary degrees of freedom generate entropic forces that stabilize a target order at finite system size through a modified free-energy landscape. Specifically, we couple topological defects to local entropic reservoirs—mesoscopic baths of auxiliary states—engineered such that the defect-free vacuum allows the reservoir to explore a large phase-space volume M , while the presence of a defect confines it to a unique state. This asymmetry produces an entropic free-energy barrier which scales intrinsically with temperature and therefore remains effective even when energetic gaps are

overwhelmed by thermal fluctuations.

We apply this framework to both discrete and continuous topological defects. In section II, to illustrate the idea, we exactly solve the entropic Ising chain and find the behavior of the correlation length to exhibit three distinct regimes as a function of temperature: linear increase, plateau and eventual breakdown. Moving on to the two-dimensional entropic toric code in section III, we analyze both the static and dynamical stabilities of the toric code ground state at finite system size and uncover a “double suppression” effect: the entropic bath not only suppresses the defect density by $\sim M^{-2}$, but also kinetically suppresses the diffusion of anyons, reducing their mobility by a factor of M^{-1} . A concrete implementation using Rydberg atom arrays generalizing the dual-species “Weimer-bath” architecture [16] is proposed in section III C. Extending the discussion to the BKT transition, we show in section IV that the entropic coupling effectively renormalizes the vortex core energy, restoring a nonzero tension to vortex worldlines and thereby pushing the crossover temperature to significantly higher values at finite system size.

Our work is strongly inspired by recent studies of entropic stabilization in equilibrium lattice systems [17], which demonstrated that coupling a system to auxiliary degrees of freedom with a large entropic capacity can evade no-go theorems forbidding long-range order or entanglement at high temperature [18, 19]. The references primarily focused on the existence of stable phases in the thermodynamic limit, emphasizing higher spatial dimensions where true finite-temperature order can persist. The present work explores a complementary and experimentally motivated regime. Rather than seeking stabilization in the two-dimensional thermodynamic limit — where topological order remains forbidden—we focus on finite-size systems, which are the natural setting for quantum memories and programmable quantum simulators. We concentrate on the kinetic and dynamical aspects of entropic protection, including defect nucleation, transport, and lifetime scaling, explicitly analyze memory stability in two spatial dimensions, and propose concrete experimental implementations. In this sense, our work provides a dynamical realization of entropic stabilization tailored to practical quantum information processing. Finally, our mechanism is distinct from the phenomenon of order by disorder [20]. In those scenarios, thermal fluctuations select a specific ordered state from a degenerate manifold by maximizing entropy within the low-energy sector. In contrast, entropic protection relies on neither intrinsic frustration nor ground-state degeneracy. Instead, entropy is engineered as an auxiliary barrier that suppresses the nucleation and motion of defects, hardening the phase against thermal erosion. While order by disorder uses entropy to select an ordered state, our mechanism uses entropy to protect it.

While not directly addressing our setup, related discussions of protected order at finite or high temperatures can also be found in Refs. [21–38].

II. THE ENTROPIC ISING CHAIN

This warm-up section considers Ising model coupled to local entropic reservoirs with dimension M . In standard ferromagnetic Ising chain, the correlation length is purely energetic, $\xi \sim e^{2\beta J}$, and diverges only at zero temperature ($\beta \rightarrow \infty$). Below we will show that entropic reservoirs generate a correlation length $\xi \propto M$ that, when M is comparable with system size L , can remain macroscopic even at high temperatures. The Hamiltonian is:

$$H = \sum_i \hat{n}_i \left(\epsilon \frac{1 + Z_i Z_{i+1}}{2} + J \frac{1 - Z_i Z_{i+1}}{2} \right). \quad (1)$$

Here, \hat{n}_i describes a local bath with M available states ($n_i = 0, 1, \dots, M - 1$). The interaction enforces a state-dependent phase space volume: If a domain wall exists ($Z_i Z_{i+1} = -1$), the bath experiences a potential via $J \hat{n}_i$. When the potential is steep $\beta J \gg 1$, the bath is confined to its ground state where $\langle \hat{n}_i \rangle = 0$. Conversely, if the stabilizer is satisfied ($Z_i Z_{i+1} = +1$), the small ϵ allows the boson to effectively delocalize over a large phase space volume in the ground sector of spins while regulating the bath states to be normalizable.

The spin correlation length can be exactly solved by integrating out the bath. The full partition function $Z = \text{Tr}(\prod T_i)$ is determined by the transfer matrix in the computational spin basis: $T = \begin{pmatrix} w_+ & w_- \\ w_- & w_+ \end{pmatrix}$, where w_{\pm} are the Boltzmann weights for the local link configurations $Z_i Z_{i+1} = \pm 1$. Since the eigenvalues of T are $w_{\pm} \pm w_-$, it’s straightforward to derive that the spin-spin correlation function, which decays as:

$$\langle Z_i Z_{i+r} \rangle = \left(\frac{w_+ - w_-}{w_+ + w_-} \right)^r. \quad (2)$$

Upon identification of the correlator with the form $e^{-r/\xi}$, one can derive the correlation length to be

$$\xi = \left[\ln \frac{\lambda + 1}{\lambda - 1} \right]^{-1}, \quad (3)$$

where λ is the ratio

$$\lambda \equiv \frac{w_+}{w_-} = \frac{1 - e^{-\beta \epsilon M}}{1 - e^{-\beta \epsilon}} \frac{1 - e^{-\beta J}}{1 - e^{-\beta JM}}. \quad (4)$$

There are three regimes with distinct physics when decreasing β , when the thermal energy is larger than ϵ . The results are summarized in fig. 1.

Inverse melting regime: $\beta \epsilon \ll 1 \ll \beta \epsilon M; \beta J \gg 1$. The thermal energy exceeds the boson level spacing ϵ , allowing the bath to behave as a thermal gas in the ground sector of spins. However, the temperature is still lower than the total energy span $M\epsilon$, so the bath does not yet feel the hard cutoff M . In this case, $w_+ \approx (\beta \epsilon)^{-1}$, while $w_- \approx 1$ is still frozen by J . The correlation length thus

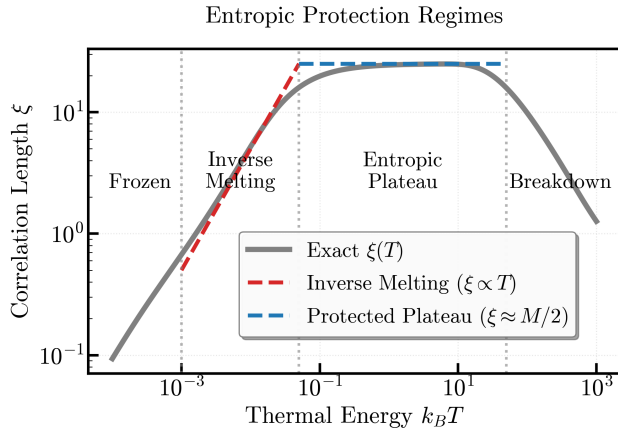


FIG. 1. Correlation length as a function of thermal energy $1/\beta$. Parameters are chosen as $M = 50$, $\epsilon = 10^{-3}$, $J = 50$.

scales as $\xi \sim (\beta\epsilon)^{-1}$, which grows linearly with temperature.

Saturated entropic plateau: $\beta\epsilon M \ll 1 \ll \beta J$. The temperature is now high enough to saturate the entire bandwidth of the bath, so all M states are equally accessible. Yet, it is still too low to overcome the defect penalty J . Now $w_+ \approx \beta\epsilon M/\beta\epsilon = M$ and $w_- \approx 1$ is still frozen. In this case, $\xi \approx M/2$. The correlation length hits a robust maximum plateau and becomes temperature independent. In the thermodynamic limit $L \rightarrow \infty$, for any fixed finite M , true long range order is absent. Nevertheless, at finite L , the system behaves as if it were Ising ordered once M is comparable to L .

Breakdown regime: $\beta J \ll 1$. When the thermal fluctuations finally exceed the defect energy J , w_+ remains saturated at M , but w_- begins to grow ($w_- > 1$) as the defect bath gets excited. Then ξ collapses as λ decreases.

We remark that at strictly zero temperature, $\beta \rightarrow \infty$, the bath is frozen into its ground state $n_i = 0$ for all spin configurations, and the Hamiltonian (1) vanishes identically. As a result, all spin configurations are exactly degenerate and the spins are completely disordered. The ordering mechanism discussed here is therefore intrinsically a finite-temperature effect, arising purely from entropic contributions to the free energy. To connect this entropically stabilized Ising physics to the conventional zero-temperature limit, one can add a direct nearest-neighbor Ising interaction, which will be discussed in Appendix A.

III. ENTROPIC PROTECTION OF 2D TORIC CODE

This section discusses the entropic protection of topological quantum memory in two dimensions. We will focus on the Toric Code [1] defined on a square lattice with periodic boundary conditions. The logical information is encoded in the degenerate ground space absent of anyonic excitations.

The system consists of gauge qubits located on the links of the lattice, coupled to bath degrees of freedom located on the vertices (v) and plaquettes (p). The Hamiltonian is given by:

$$H = \frac{1}{2} \sum_v \left[J(1 - \hat{A}_v) \hat{n}_v + \epsilon(1 + \hat{A}_v) \hat{n}_v \right] \quad (5)$$

$$\frac{1}{2} \sum_p \left[J(1 - \hat{B}_p) \hat{n}_p + \epsilon(1 + \hat{B}_p) \hat{n}_p \right].$$

The standard toric code stabilizers are $\hat{A}_v = \prod_{j \ni v} X_j$ and $\hat{B}_p = \prod_{j \in p} Z_j$. The operators $\hat{n}_{v,p}$ represent the coupling to local entropic reservoirs.

While an inverse melting regime is also present similar to the Ising case in II, we will focus on the saturated entropic regime, $\beta\epsilon M \ll 1 \ll \beta J$, where the correlation physics is independent of temperature. In this window, the partition function for a local reservoir is $w_+ \approx M$ if the stabilizer is satisfied, and $w_- \approx 1$ if it is violated. This generates an effective free energy cost for anyons: the probability ratio of a state with a single anyon pair to the ground state is: $(w_-/w_+)^2 \approx M^{-2}$, which corresponds to an entropic free energy cost of $\beta^{-1} \ln M$ violated stabilizer. Unlike energetic gaps which are fixed constants, this chemical potential scales linearly with temperature, maintaining a constant suppression of anyon density even as T increases.

A. Static stability

To quantify the preservation of topological order in the Gibbs state $\rho(T) = e^{-\beta H}/Z$, this section computes the scaling of Wilson loops as well as the topological entanglement entropy.

The Wilson loop is defined as usual $W_z(R) = \prod_{p \in R} B_p$ surrounding a region R . In the regime of saturated entropic plateau, the expectation value for a single B_p is $\langle B_p \rangle = (w_+ - w_-)/(w_+ + w_-) \sim 1 - 2/M$ when expanded in large M . The scaling of the wilson loop is thus

$$\langle W_z(R) \rangle = \prod_{p \in R} \langle B_p \rangle \sim e^{|R| \ln(1 - 2/M)}. \quad (6)$$

Note that the logarithm is always negative. Therefore, the Wilson loop is area-law decaying except when $M \rightarrow \infty$, which strictly speaking indicates confinement at any finite M . However, we emphasize that neither β nor system size N enters the expression. While strictly this implies a confined phase, the entropic confinement is nontrivial and fundamentally different from standard thermal destabilization, as the effective string tension is temperature-independent and can be arbitrarily suppressed by increasing the bath dimension M rather than cooling the system.

Next we examine the topological entanglement entropy [39, 40] which by construction cancels out classical correlations and can serve as a diagnosis for topological order

at finite temperature. For each toric code stabilizer S of type either \hat{A}_v or \hat{B}_p , the local density matrix after tracing out the corresponding bosons \hat{n}_S reads,

$$\rho_S \propto \frac{1+S}{2} \frac{1-e^{-\beta\epsilon M}}{1-e^{-\beta\epsilon}} + \frac{1-S}{2} \frac{1-e^{-\beta JM}}{1-e^{-\beta J}}. \quad (7)$$

Such density matrix can be identified with the thermal density matrix of standard toric code $\rho_S = Ce^{\beta_{\text{eff}} S}$, where

$$\beta_{\text{eff}} = \frac{1}{2} \ln \frac{(1-e^{-\beta\epsilon M})(1-e^{-\beta J})}{(1-e^{-\beta\epsilon})(1-e^{-\beta JM})}. \quad (8)$$

This establishes a direct mapping to the finite-temperature toric code, whose topological entanglement entropy vanishes at any non-zero temperature [2] in the thermodynamic limit. For a finite system with N sites, the topological correction to the entropy remains robust only when $\sqrt{N}e^{-\beta_{\text{eff}}} \ll 1$. In our saturated entropic plateau regime, where $\beta_{\text{eff}} \sim \frac{1}{2} \ln M$, this implies a threshold condition for the bath size of $M \sim N$. Notably, M is the Hilbert space dimension of the bath - if the bath contains m qubits, the number of qubits required for each bath only needs to scale with the logarithm of the number of system qubits

$$m \sim \log_2 N. \quad (9)$$

While this scaling implies that m must diverge in the thermodynamic limit to preserve equilibrium order, this is not a practical bottleneck for quantum information processing. For a realistic fault-tolerant memory patch with system size $N = 250$, the required bath degrees of freedom $m \approx 8$ is within the reach of current experimental platforms, such as multi-level Rydberg states or small clusters of atoms exploiting hyperfine manifolds. We will describe a possible experimental proposal in section III C.

B. Dynamic Stability

The lifetime of the quantum memory depends on dynamical coupling to external environment, which we will examine using a Lindblad master equation:

$$\begin{aligned} \dot{\rho} = \Gamma_0 \sum_l & \left(\frac{1}{M^2} \mathcal{D}[L_{\text{cr},X_l}] + \frac{1}{M} (\mathcal{D}[L_{\text{dif},X_l}^{\rightarrow 1}] + \mathcal{D}[L_{\text{dif},X_l}^{\rightarrow 2}]) \right. \\ & \left. + \mathcal{D}[L_{\text{ann},X_l}] + (X_l \rightarrow Z_l) \right) \rho. \end{aligned} \quad (10)$$

Here $\mathcal{D}[L]\rho = L\rho L^\dagger - \frac{1}{2}\{L^\dagger L, \rho\}$ and the jump operators L 's can be expressed by local Pauli operator X_l and Z_l 's, as well as A_v , B_p projectors, see Appendix B for detailed derivation of (10). This master equation reveals a distinct hierarchy of transition rates:

Pair Creation. The term $\mathcal{D}[L_{\text{cr}}]$ describes the nucleation of a defect pair from the vacuum. This process requires two local reservoirs to spontaneously fluctuate

from the flat sector (volume M) into the confined sector (volume 1), incurring a rate penalty $\Gamma_{\text{cr}} \sim M^{-2}$.

Anyon Diffusion. The terms $\mathcal{D}[L_{\text{dif}}]$ describe the hopping of an anyon to an adjacent site. While energetically neutral, this transport is kinetically gated. The reservoir at the target site must fluctuate into a specific microstate to accept the defect, reducing the effective diffusion constant to $D_{\text{eff}} \sim D_0 M^{-1}$.

Pair Annihilation. The process $\mathcal{D}[L_{\text{ann}}]$ relaxes the baths into the high-entropy vacuum sector and is therefore entropically uninhibited, proceeding at the bare rate Γ_0 .

A key question for passive quantum memory is how the lifetime of the logical information depends on the linear system size $L = \sqrt{N}$ and on the entropic reservoir dimension M . A logical error occurs when the pair of anyons created wind around a non-contractible loop of the torus before getting annihilated again. In the saturated entropic regime $\beta\epsilon M \ll 1 \ll \beta J$, the steady-state defect density is parametrically suppressed as $n = \Gamma_{\text{cr}}/\Gamma_{\text{ann}} \sim M^{-2}$, such that the typical anyon separation is, in lattice units, $\ell = n^{-1/2} \sim M$.

(i) *Defect-rare regime.* Assuming static stability which requires $M \gg 1$ to scale at least as L^2 , the ratio $L/\ell \sim 1/L \ll 1$ and we are naturally in the regime where the defects are rare. The total rate to nucleate a pair anywhere scales with the volume $P_{\text{cr}} = L^2 \Gamma_{\text{cr}} \sim \Gamma_0 L^2/M^2$. Once created, the pair undergoes a two-dimensional random walk with diffusion constant $\sim D_{\text{eff}}$. For a nontrivial winding to happen, the pair must separate to a distance of order L with probability $\sim 1/\ln L$. The logical lifetime is then the inverse of the creation-winding probability:

$$\tau_L \sim M^2 \ln L / \Gamma_0 L^2 \quad (11)$$

which scales at least as $L^2 \ln L$.

(ii) *Finite anyon density.* For sufficiently large systems $L \gg \ell$, many anyons coexist at steady state. The rate for a given anyon to contribute a nontrivial winding is set by the spectral gap of diffusion ($\partial_t n^2 = D_{\text{eff}} \nabla^2 n$) on a torus, $\sim D_{\text{eff}}/L^2$. Multiplying by the number of anyons $\sim nL^2$ gives the logical error rate $\tau_L^{-1} \sim (nL^2)(D_{\text{eff}}/L^2) \sim D_0/M^3$, and hence

$$\tau_L \sim M^3 / D_0. \quad (12)$$

Importantly, the lifetime does not grow with L in the thermodynamic limit: the mechanism enhances the memory time only parametrically through M (by suppressing both the defect density and defect mobility), consistent with no-go results in two dimensions.

It is instructive to compare this result with the standard toric code, where protection arises purely from an energy gap Δ . In that case, the memory lifetime follows the Arrhenius law $\tau_{\text{std}} \sim \tau_0 \exp(\beta\Delta)$, which is extremely sensitive to thermal fluctuations.

C. Experimental setup

We propose a concrete implementation using a dual-species Rydberg atom array (e.g., ^{87}Rb for system qubits living on the links and ^{133}Cs for bath atoms living on the vertices and plaquette centers) [41]. A central challenge is implementing the conditional Hamiltonian term which applies a steep penalty to the bath only when the 4-body stabilizer is violated. To bridge the locality gap between the system stabilizer and the bath potential, a single auxiliary sensor atom (Cs) needs to be introduced at the center of each plaquette and vertex (in addition to the bath atoms), serving as a mediator. The protocol operates in a hybrid digital-analog regime:

(i) *Stabilizer Mapping.* We utilize the standard ancilla-based stabilizer-measurement circuit, in which the parity of four data qubits is mapped onto a sensor atom via four ancilla-data entangling operations (equivalent to four CNOT or CZ gates at the logical level [8]). In Rydberg-atom platforms, such coupling are implemented using native blockade-based pulse sequences rather than explicit two-qubit gates, following the general schemes introduced in [16, 42] and demonstrated experimentally in [43–45]. If the stabilizer is satisfied (+1), the sensor will remain in the ground state $|g\rangle$. If violated (−1), the sensor will flip to a metastable clock state $|e\rangle$.

(ii) *Conditional Blockade.* To generate the steep defect penalty J , we use the technique of Rydberg dressing [46, 47]. We propose to apply an off-resonant laser field that couples the sensor’s excited state $|e\rangle$ (and consequently the Bath atoms) to a high-lying Rydberg state $|r\rangle$. This laser does not fully excite the atoms to the Rydberg state (which would decay too quickly); instead, it dresses the ground state by mixing in a small fraction of Rydberg character. This small fraction is sufficient to induce strong van der Waals interactions between the sensor and the bath, creating the steep energy penalty J . Crucially, if the sensor is in the ground state $|g\rangle$, the laser is far off-resonance, the Rydberg mixing is negligible, and the Bath remains non-interacting (shallow $\epsilon \approx 0$). The setup is demonstrated in fig. 2.

The defect penalty J is set by the strength of the Rydberg-dressed interaction between the sensor and bath atoms. For example, the spin-flip blockade in [48] was able to realize defect penalty $\sim 1\text{MHz}$ in units of Planck constant. The residual conditional coupling from far-detuned Rydberg dressing is strongly suppressed, yielding $\epsilon/h \sim 10\text{ kHz}$ for typical parameters. The effective temperature $k_B T$ is set primarily by the motional temperature of laser-cooled atoms and control-field noise; values $T \sim 10\mu\text{K}$ (take [49] as an example), corresponding to $k_B T/h \sim 200\text{kHz}$, are typical. These scales can be arranged to satisfy the hierarchy $\epsilon \ll k_B T \ll J$. We remark that while our low temperature requirement to reach the desired code sector is similar to that of other existing state-preparation methods, this alone does not protect against coherent control errors and noise-induced defect diffusion. The entropic stabilization mechanism

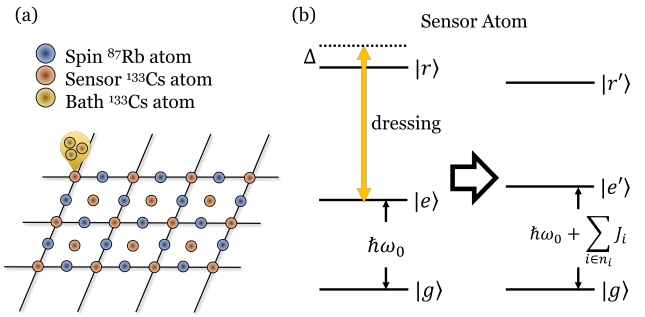


FIG. 2. (a) Schematic of the proposed dual-species Rydberg atom array, which consists of target spins (blue, ^{87}Rb), sensor atoms (red, ^{133}Cs), and bath atoms (yellow, ^{133}Cs). Each sensor serves as a messenger between the system lattice and a local entropic reservoir formed by the bath cluster. (b) Conditional blockade via Rydberg dressing. The relevant energy levels $|g\rangle$, $|e\rangle$, and $|r\rangle$ correspond to the ground, excited, and Rydberg states of the Cs atoms. An off-resonant laser with Rabi frequency Ω and negative detuning $|\Delta| \gg \Omega$ dresses the excited state, creating $|e'\rangle$ with a small admixture of Rydberg $|r\rangle$. This induces strong van der Waals interactions $\propto J_i$ between the sensor and surrounding bath atom i . The resulting total energy shift, $\sum J_i$, enforces the energetic penalty for defects. Crucially, the entropic stabilization relies on the degenerate bath configurations rather than precise energy matching, making the protocol robust against variations in interaction strengths J_i arising from different inter-atomic distances R_i between the bath and sensor atoms.

suppresses logical error processes after preparation, removing the need for continuous active error correction on experimental timescales.

IV. ENTROPIC PROTECTION OF SUPERFLUIDS

Having demonstrated the stabilization of discrete topological memory, we now extend the framework to continuous variables by considering the two-dimensional XY model coupled to entropic reservoirs. The physics here is governed by the binding and unbinding of vortex defects, described by the Berezinskii–Kosterlitz–Thouless (BKT) transition.

Consider a square lattice of planar rotors $\theta_i \in [0, 2\pi)$. The standard XY interaction is dressed by a coupling to local baths located on the plaquettes p . The full Hamiltonian is

$$H = -J \sum_{\langle ij \rangle} \cos(\theta_i - \theta_j) + \sum_p H_p^{\text{bath}}(\Phi_p), \quad (13)$$

where $\Phi_p = \sum_{\square} (\theta_i - \theta_j)$ denotes the vorticity around plaquette p , defined using the usual convention that angular differences are taken modulo 2π . The bath term H_p^{bath} imposes an entropic penalty on nonzero vorticity.

We assume the saturated entropic plateau regime: when $\Phi_p = 0$, the local bath has volume M , while for

$\Phi_p \neq 0$ the bath is confined to a single microstate. A single vortex incurs the standard energetic core cost E_c , together with an additional entropic cost due to the collapse of the bath phase space. Integrating out the bath degrees of freedom generates an effective free-energy cost $\Delta F = E_c + \beta^{-1} \ln M$. In the renormalization-group analysis, the relevant control parameter is the vortex fugacity, which is renormalized by the bath from the bare value to $y_0 = e^{-\beta E_c}$ to

$$y_{\text{eff}} = y_0/M. \quad (14)$$

Let $K = \beta J$ denote the stiffness. To leading order, the RG flow equations read

$$\frac{dK^{-1}}{dl} = 4\pi^3 y^2 + \dots, \quad \frac{dy}{dl} = (2 - \pi K)y + \dots. \quad (15)$$

In the limit of small bare fugacity, these equations imply that vortices become relevant when the stiffness approaches $K \simeq 2/\pi$. In our entropic setup (13), the initial condition for the flow is modified to $y(l=0) = y_0/M$. For $y_0/M \ll 1$, there is an initial linear stage of the flow on the disordered side ($\beta < \beta_{\text{BKT}}$) where $K(l)$ varies slowly as visible from the RG equation. Approximating $K(l) \approx K$ over this stage gives $y(l) \approx y(0) e^{(2-\pi K)l}$, so the scale l^* at which vortices proliferate ($y(l^*) \sim O(1)$) shifts by $\Delta l^* \equiv l_{\text{eff}}^* - l_0^* \simeq (2 - \pi K)^{-1} \ln M$. Since $\xi \sim a e^{l^*}$, this yields an additional multiplicative enhancement of the correlation length,

$$\xi \simeq \xi_0 M^{\nu_{\text{eff}}}, \quad \nu_{\text{eff}}(\beta) = \frac{1}{2 - \pi K}, \quad (16)$$

valid in the regime where the linearized flow controls the onset of vortex proliferation, i.e., before the asymptotic critical scaling regime sets in. Here ξ_0 denotes the correlation length without entropic coupling, which near the transition diverges as $\ln \xi_0 \sim b/\sqrt{\beta_{\text{BKT}}/\beta - 1}$.

In a finite system, global phase coherence is lost at a crossover scale $\beta_c(L)$ determined by the condition $\xi(\beta_c) \sim L$. In the standard XY model this crossover occurs slightly below the BKT transition β_{BKT} . In the presence of entropic stabilization, the correlation length is parametrically enhanced over a broad temperature window away from the asymptotic critical regime, which in turn shifts the finite-size crossover to smaller β (higher temperature). At the level of scaling, this implies

$$\frac{\beta_{\text{BKT}}}{\beta_c} \simeq 1 + \left(\frac{b}{\ln L - \nu_{\text{eff}} \ln M} \right)^2 \quad (17)$$

with the understanding that $\beta_c(L)$ denotes a finite-size coherence crossover rather than a true critical point. Consequently, for sufficiently large bath entropy, phase coherence can persist well above the bare BKT scale in finite systems.

Finally, vortex dynamics are suppressed by the similar entropic mechanism discussed for the toric code. A vortex hop to a neighboring plaquette requires the target

reservoir to fluctuate into the specific microstate compatible with the vortex core, which kinetically gates vortex motion and reduces the effective diffusion constant to $D_{\text{eff}} \sim D_0/M$. The rate of phase-slip processes—which require the creation and separation of vortex–antivortex pairs—therefore scales as

$$\Gamma_{\text{slip}} \sim y_{\text{eff}} D_{\text{eff}} \propto M^{-2},$$

up to nonuniversal prefactors. This combined suppression of vortex density and mobility provides a dynamical complement to the thermodynamic enhancement of the correlation length.

V. DISCUSSION AND OUTLOOK

We have shown that entropy, typically the adversary of quantum order, can be engineered to serve as its protector. By creating a landscape where topological defects are entropically confined, in finite systems one can achieve a polynomial enhancement in toric code memory lifetime even in the finite-anyon density regime ($\tau \sim M^3$) and a significant expansion of superfluid coherence (slip error rate $\sim M^{-2}$). This mechanism offers a new, resource-efficient paradigm for stabilizing quantum matter in the noisy intermediate-scale era.

Here we comment more on the experimental setup of entropic toric code in section III C. The primary advantage of this setup is the exponential resource scaling. Using a modest bath of $m = 7$ atoms can already yield a Hilbert-space dimension $M = 2^m = 128$, giving an entropic suppression factor $M^3 \simeq 2.1 \times 10^6$. Furthermore, the parameters J and ϵ are optically tunable, allowing dynamic exploration of the phase diagram and the breakdown transition.

A practical limitation of the proposed implementation is the finite coherence time associated with Rydberg dressing. While entropic protection suppresses the generation and transport of logical errors, the protection itself is ultimately limited by photon scattering from the dressing lasers and by the effective lifetime of the weakly mixed Rydberg states, typically in the range of 10–100 ms [47]. This finite lifetime is not unique to our setup but reflects a general constraint of Rydberg-based implementations; indeed, the timescale achievable with Rydberg dressing is often longer than the coherence window in experiments based on resonant Rydberg blockade. Another limitation is that the scheme relies on the fidelity of the digital stabilizer-mapping step that conditions the bath potential on the stabilizer eigenvalue. Imperfections in gate operations or sensor readout effectively introduce leakage channels that reduce the entropic barrier. Encouragingly, recent Rydberg experiments have demonstrated multi-qubit parity and stabilizer-mapping fidelities above the 99% level (see for example [50, 51]), indicating that this requirement is compatible with current capabilities.

An intriguing direction for future work is the hybridization of passive entropic protection with active quantum

error correction. In conventional active schemes, a decoder must identify and correct errors faster than they accumulate, requiring the physical error rate to lie below a threshold $p < p_c$. Entropic protection can be viewed as a hardware-level pre-filter that renormalizes the effective rate of dangerous error processes. Operating a standard decoder on top of an entropically protected substrate could therefore enable fault tolerance using significantly noisier physical components.

More broadly, this work also raises the question of whether entropic baths can be used to stabilize conformal critical points at finite temperature. For example in the transverse-field Ising chain, the critical point is governed at zero temperature by the Ising conformal field theory, while finite temperature normally produces a quantum critical fan rather than a true critical state. It would be interesting to explore whether an entropic bath can effectively counteract thermal decoherence and preserve conformal scaling over extended length and time scales. Such scenarios would represent a qualitatively new form of bath-stabilized criticality, which may be related to the investigations in Refs. [24–37].

ACKNOWLEDGMENTS

We thank Yiqiu Han for introducing her work, Itamar Kimchi and Xueda Wen for discussions related to Appendix A, and Google Gemini 3 Pro for inspiring conversations. This research was supported in part by grant NSF PHY-2309135 to the Kavli Institute for Theoretical Physics (KITP).

Appendix A: Modified Ising chain

In this Appendix, we connect the entropic stabilization physics (1) to that of the conventional Ising chain by adding

$$H' = H - J' \sum_i Z_i Z_{i+1}. \quad (\text{A1})$$

This term does not modify the structure of the transfer-matrix solution, but simply renormalizes the ratio (4) as

$$\lambda' = \lambda e^{2\beta J'}. \quad (\text{A2})$$

Consequently, the correlation length becomes

$$\xi' = \left[\ln \frac{\lambda' + 1}{\lambda' - 1} \right]^{-1}. \quad (\text{A3})$$

In the low temperature limit $\beta \rightarrow \infty$, the additional exponential factor $e^{2\beta J'}$ becomes enormous, such that ξ' diverges as expected in the standard Ising model. At higher temperatures, as long as $\beta J'$ is small compared with other scales in the system, the entropic plateau region is still intact. In fig. 3, we plot the correlation length plateau as a function of J' and thermal energy.

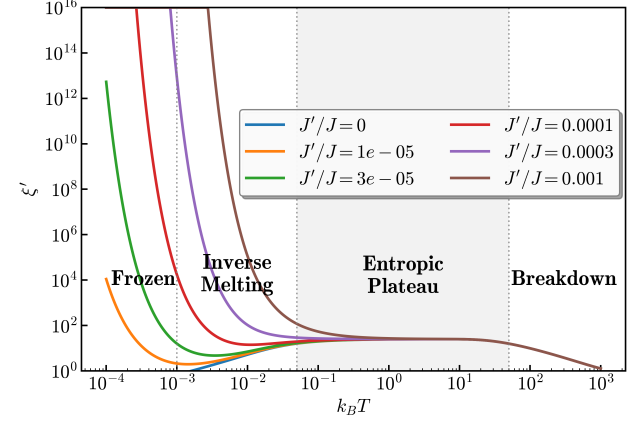


FIG. 3. Correlation length as a function of thermal energy for different values of J' .

Appendix B: Microscopic Derivation of Entropic Lindbladian

In this appendix, we derive the effective Lindblad master equation governing the memory dynamics. We start from the microscopic Hamiltonian of the toric code coupled to local entropic reservoirs and perform an adiabatic elimination of the bath degrees of freedom under the assumption of weak system–bath coupling. We model physical error processes as a weak coupling between the system qubits and an external, unbounded environment, mediated by single-qubit operators. The interaction Hamiltonian is

$$V = \sum_l (X_l \otimes \mathcal{E}_l^x + Z_l \otimes \mathcal{E}_l^z), \quad (\text{B1})$$

where $\mathcal{E}_l^{x,z}$ are operators acting on the external environment. We treat this perturbatively using Fermi's Golden Rule to derive transition rates between stabilizer configurations. Crucially, the interaction acts only on the system qubits and leaves the local entropic bath states unchanged.

Consider a transition from a stabilizer configuration s to s' induced by a bit-flip X_l . The corresponding transition rate is

$$\Gamma_{s \rightarrow s'} = \Gamma_0 \sum_{\{n\}_{s'}, \{n\}_s} \mathcal{P}(\{n\}_s) |\langle \{n\}_{s'} | \langle s' | X_l | s \rangle | \{n\}_s \rangle|^2, \quad (\text{B2})$$

where Γ_0 is the bare transition rate and $\mathcal{P}(\{n\}_s)$ denotes the thermal probability of finding the bath configuration $\{n\}$ conditioned on the stabilizer configuration s . Since X_l acts trivially on the bath degrees of freedom, the matrix element is nonzero only if the bath configuration is conserved, $\{n\}_{s'} = \{n\}_s$. Consequently, the transition rate is determined by the probability that a thermal bath configuration compatible with s remains a valid eigenstate of the bath Hamiltonian associated with s' .

a. *Pair creation.* Both plaquettes p_1 and p_2 initially lie in the target sector ($B_p = +1$) and are flipped into the

defect sector ($B_p = -1$). In the entropic plateau regime, the initial bath configurations are uniformly distributed, so that $\mathcal{P}(n_{p_1}, n_{p_2}) \approx M^{-2}$. In the final configuration, the steep potential enforces $n_{p_1} = n_{p_2} = 0$; any other configuration incurs an energetic penalty J . The transition is therefore resonant only if the initial bath configuration already satisfies this constraint, yielding a pair-creation rate

$$\Gamma_{\text{cr}} \approx \Gamma_0 M^{-2}. \quad (\text{B3})$$

b. *Anyon diffusion.* This process corresponds to one plaquette p_1 relaxing ($- \rightarrow +$) while the neighboring plaquette p_2 is excited ($+ \rightarrow -$). The initial bath probability is $\mathcal{P}(0, n_{p_2}) \approx M^{-1}$. After the hop, the bath at p_1 experiences a flat potential, while the bath at p_2 must satisfy $n_{p_2} = 0$. The resulting diffusion rate is

$$\Gamma_{\text{dif}} \approx \Gamma_0 M^{-1}. \quad (\text{B4})$$

c. *Pair annihilation.* In this process both plaquettes relax back to the vacuum sector. Initially, the baths are frozen at $(n_{p_1}, n_{p_2}) = (0, 0)$ with probability $\mathcal{P}(0, 0) \approx 1$. In the final configuration, the potential is flat and all bath states are allowed, so the annihilation rate is unsuppressed:

$$\Gamma_{\text{ann}} \approx \Gamma_0. \quad (\text{B5})$$

Although physical noise acts uniformly on all links, the entropic reservoirs selectively filter these events depending on the instantaneous stabilizer configuration. To capture this state-dependent dynamics, we decompose the bit-flip operator X_l acting on the link shared by plaquettes p_1 and p_2 into transition operators between specific stabilizer subspaces. We define projectors onto the vacuum (target) and defect (error) subspaces of a plaquette

p as

$$\Pi_p^+ = \frac{1 + B_p}{2}, \quad \Pi_p^- = \frac{1 - B_p}{2}. \quad (\text{B6})$$

The operator X_l can then be decomposed into three distinct jump operators corresponding to the three processes discussed above:

$$\begin{aligned} L_{\text{cr}, X_l} &= X_l \Pi_{p_1}^+ \Pi_{p_2}^+ = \Pi_{p_1}^- \Pi_{p_2}^- X_l, \\ L_{\text{dif}, X_l}^{\rightarrow 1} &= X_l \Pi_{p_1}^- \Pi_{p_2}^+, \quad L_{\text{dif}, X_l}^{\rightarrow 2} = X_l \Pi_{p_1}^+ \Pi_{p_2}^-, \\ L_{\text{ann}, X_l} &= X_l \Pi_{p_1}^- \Pi_{p_2}^- = \Pi_{p_1}^+ \Pi_{p_2}^+ X_l. \end{aligned} \quad (\text{B7})$$

The total effective Lindbladian is obtained by summing over all links l (and analogously including Z_l errors on the vertices):

$$\begin{aligned} \dot{\rho} = \sum_l & \left(\Gamma_{\text{cr}} \mathcal{D}[L_{\text{cr}, X_l}] + \Gamma_{\text{dif}} (\mathcal{D}[L_{\text{dif}, X_l}^{\rightarrow 1}] + \mathcal{D}[L_{\text{dif}, X_l}^{\rightarrow 2}]) \right. \\ & \left. + \Gamma_{\text{ann}} \mathcal{D}[L_{\text{ann}, X_l}] + (X_l \rightarrow Z_l) \right) \rho, \end{aligned} \quad (\text{B8})$$

where $\mathcal{D}[L]\rho = L\rho L^\dagger - \frac{1}{2}\{L^\dagger L, \rho\}$. Note that when replacing $X_l \rightarrow Z_l$, the projectors are correspondingly replaced by $\Pi_v^\pm = (1 \pm A_v)/2$. Substituting the rates derived above yields the final master equation,

$$\begin{aligned} \dot{\rho} = \Gamma_0 \sum_l & \left(\frac{1}{M^2} \mathcal{D}[L_{\text{cr}, X_l}] + \frac{1}{M} (\mathcal{D}[L_{\text{dif}, X_l}^{\rightarrow 1}] + \mathcal{D}[L_{\text{dif}, X_l}^{\rightarrow 2}]) \right. \\ & \left. + \mathcal{D}[L_{\text{ann}, X_l}] + (X_l \rightarrow Z_l) \right) \rho. \end{aligned} \quad (\text{B9})$$

This form makes explicit the hierarchy of timescales induced by the entropic reservoirs.

[1] A. Kitaev, Fault-tolerant quantum computation by anyons, *Annals of Physics* **303**, 2 (2003).

[2] C. Castelnovo and C. Chamon, Entanglement and topological entropy of the toric code at finite temperature, *Phys. Rev. B* **76**, 184442 (2007).

[3] Z. Nussinov and G. Ortiz, Autocorrelations and thermal fragility of anyonic loops in topologically quantum ordered systems, *Phys. Rev. B* **77**, 064302 (2008).

[4] B. J. Brown, D. Loss, J. K. Pachos, C. N. Self, and J. R. Wootton, Quantum memories at finite temperature, *Rev. Mod. Phys.* **88**, 045005 (2016).

[5] J. M. Kosterlitz and D. J. Thouless, Ordering, metastability and phase transitions in two-dimensional systems, *Journal of Physics C: Solid State Physics* **6**, 1181 (1973).

[6] P. W. Shor, Scheme for reducing decoherence in quantum computer memory, *Phys. Rev. A* **52**, R2493 (1995).

[7] E. Dennis, A. Kitaev, A. Landahl, and J. Preskill, Topological quantum memory, *Journal of Mathematical Physics* **43**, 4452–4505 (2002).

[8] D. Gottesman, *Stabilizer codes and quantum error correction* (California Institute of Technology, 1997).

[9] B. M. Terhal, Quantum error correction for quantum memories, *Rev. Mod. Phys.* **87**, 307 (2015).

[10] R. Alicki, M. Horodecki, P. Horodecki, and R. Horodecki, On thermal stability of topological qubit in kitaev's 4d model, *Open Systems & Information Dynamics* **17**, 1 (2010), <https://doi.org/10.1142/S1230161210000023>.

[11] J. Haah, Local stabilizer codes in three dimensions without string logical operators, *Phys. Rev. A* **83**, 042330 (2011).

[12] S. Bravyi and J. Haah, Energy landscape of 3d spin hamiltonians with topological order, *Phys. Rev. Lett.* **107**, 150504 (2011).

[13] M. Ippoliti, L. Mazza, M. Rizzi, and V. Giovannetti, Perturbative approach to continuous-time quantum error correction, *Phys. Rev. A* **91**, 042322 (2015).

[14] K. Fujii, M. Negoro, N. Imoto, and M. Kitagawa, Measurement-free topological protection using dissipative feedback, *Phys. Rev. X* **4**, 041039 (2014).

[15] M. Sarovar and G. J. Milburn, Continuous quantum error

correction by cooling, *Phys. Rev. A* **72**, 012306 (2005).

[16] H. Weimer, M. Müller, I. Lesanovsky, P. Zoller, and H. P. Büchler, A rydberg quantum simulator, *Nature Physics* **6**, 382 (2010).

[17] Y. Han, X. Huang, Z. Komargodski, A. Lucas, and F. K. Popov, Entropic order (2025), arXiv:2503.22789 [cond-mat.stat-mech].

[18] M. Kliesch, C. Gogolin, M. J. Kastoryano, A. Riera, and J. Eisert, Locality of temperature, *Phys. Rev. X* **4**, 031019 (2014).

[19] A. Bakshi, A. Liu, A. Moitra, and E. Tang, High-temperature gibbs states are unentangled and efficiently preivable (2025), arXiv:2403.16850 [quant-ph].

[20] J. Villain, R. Bidaux, J.-P. Carton, and R. Conte, Order as an effect of disorder, *Journal de Physique* **41**, 1263 (1980).

[21] M. Plazanet, C. Floare, M. R. Johnson, R. Schweins, and H. P. Trommsdorff, Freezing on heating of liquid solutions, *The Journal of Chemical Physics* **121**, 5031 (2004).

[22] L. Radzhovskiy, E. Frey, and D. R. Nelson, Novel phases and reentrant melting of two-dimensional colloidal crystals, *Phys. Rev. E* **63**, 031503 (2001).

[23] L. Goldstein, On the theory of liquid and solid he_3 , *Annals of Physics* **8**, 390 (1959).

[24] N. Chai, S. Chaudhuri, C. Choi, Z. Komargodski, E. Rabinovici, and M. Smolkin, Symmetry breaking at all temperatures, *Phys. Rev. Lett.* **125**, 131603 (2020).

[25] N. Chai, S. Chaudhuri, C. Choi, Z. Komargodski, E. Rabinovici, and M. Smolkin, Thermal order in conformal theories, *Phys. Rev. D* **102**, 065014 (2020).

[26] P. Liendo, J. Rong, and H. Zhang, Spontaneous breaking of finite group symmetries at all temperatures, *SciPost Phys.* **14**, 168 (2023).

[27] N. Chai, E. Rabinovici, R. Sinha, and M. Smolkin, The bi-conical vector model at $1/n$, *Journal of High Energy Physics* **2021**, 10.1007/jhep05(2021)192 (2021).

[28] S. Chaudhuri and E. Rabinovici, Symmetry breaking at high temperatures in large n gauge theories, *Journal of High Energy Physics* **2021**, 10.1007/jhep08(2021)148 (2021).

[29] B. Bajc, A. Lugo, and F. Sannino, Asymptotically free and safe fate of symmetry nonrestoration, *Phys. Rev. D* **103**, 096014 (2021).

[30] P. Agrawal and M. Nee, Avoided deconfinement in randall-sundrum models, *Journal of High Energy Physics* **2021**, 10.1007/jhep10(2021)105 (2021).

[31] B. Hawashin, J. Rong, and M. M. Scherer, Ultraviolet-complete local field theory of persistent symmetry breaking in $2 + 1$ dimensions, *Phys. Rev. Lett.* **134**, 041602 (2025).

[32] Z. Komargodski and F. K. Popov, Temperature-resistant order in $2 + 1$ dimensions, *Phys. Rev. Lett.* **135**, 091602 (2025).

[33] A. Buchel, Fate of the conformal order, *Phys. Rev. D* **103**, 026008 (2021).

[34] A. Buchel, Thermal order in holographic cfts and no-hair theorem violation in black branes, *Nuclear Physics B* **967**, 115425 (2021).

[35] A. Buchel, Compactified holographic conformal order, *Nuclear Physics B* **973**, 115605 (2021).

[36] A. Buchel, Holographic conformal order with higher derivatives, *Nuclear Physics B* **1004**, 116578 (2024).

[37] N. Chai, A. Dymarsky, M. Goykhman, R. Sinha, and M. Smolkin, A model of persistent breaking of continuous symmetry, *SciPost Phys.* **12**, 181 (2022).

[38] S.-T. Zhou, M. Cheng, T. Rakovszky, C. von Keyserlingk, and T. D. Ellison, Finite-temperature quantum topological order in three dimensions, *Phys. Rev. Lett.* **135**, 040402 (2025).

[39] A. Kitaev and J. Preskill, Topological entanglement entropy, *Phys. Rev. Lett.* **96**, 110404 (2006).

[40] M. Levin and X.-G. Wen, Detecting topological order in a ground state wave function, *Phys. Rev. Lett.* **96**, 110405 (2006).

[41] I. I. Beterov and M. Saffman, Rydberg blockade, förster resonances, and quantum state measurements with different atomic species, *Phys. Rev. A* **92**, 042710 (2015).

[42] M. Müller, S. Diehl, G. Pupillo, and P. Zoller, Engineered open systems and quantum simulations with atoms and ions, in *Advances in Atomic, Molecular, and Optical Physics*, Advances In Atomic, Molecular, and Optical Physics, Vol. 61, edited by P. Berman, E. Arimondo, and C. Lin (Academic Press, 2012) pp. 1–80.

[43] H. Levine, A. Keesling, G. Semeghini, A. Omran, T. T. Wang, S. Ebadi, H. Bernien, M. Greiner, V. Vuletić, H. Pichler, and M. D. Lukin, Parallel implementation of high-fidelity multiqubit gates with neutral atoms, *Phys. Rev. Lett.* **123**, 170503 (2019).

[44] I. S. Madjarov, J. P. Covey, A. L. Shaw, J. Choi, A. Kale, A. Cooper, H. Pichler, V. Schkolnik, J. R. Williams, and M. Endres, High-fidelity entanglement and detection of alkaline-earth rydberg atoms, *Nature Physics* **16**, 857–861 (2020).

[45] P. Scholl, M. Schuler, H. J. Williams, A. A. Eberharter, D. Barredo, K.-N. Schymik, V. Lienhard, L.-P. Henry, T. C. Lang, T. Lahaye, A. M. Läuchli, and A. Browaeys, Quantum simulation of 2d antiferromagnets with hundreds of rydberg atoms, *Nature* **595**, 233–238 (2021).

[46] J. E. Johnson and S. L. Rolston, Interactions between rydberg-dressed atoms, *Phys. Rev. A* **82**, 033412 (2010).

[47] N. Henkel, R. Nath, and T. Pohl, Three-dimensional roton excitations and supersolid formation in rydberg-excited bose-einstein condensates, *Phys. Rev. Lett.* **104**, 195302 (2010).

[48] Y.-Y. Jau, A. M. Hankin, T. Keating, I. H. Deutsch, and G. W. Biedermann, Entangling atomic spins with a rydberg-dressed spin-flip blockade, *Nature Physics* **12**, 71–74 (2015).

[49] P. Scholl, M. Schuler, H. J. Williams, A. A. Eberharter, D. Barredo, K.-N. Schymik, V. Lienhard, L.-P. Henry, T. C. Lang, T. Lahaye, A. M. Läuchli, and A. Browaeys, Quantum simulation of 2d antiferromagnets with hundreds of rydberg atoms, *Nature* **595**, 233 (2021).

[50] Y. Zhao, Y. Ye, H.-L. Huang, Y. Zhang, D. Wu, H. Guan, Q. Zhu, Z. Wei, T. He, S. Cao, F. Chen, T.-H. Chung, H. Deng, D. Fan, M. Gong, C. Guo, S. Guo, L. Han, N. Li, S. Li, Y. Li, F. Liang, J. Lin, H. Qian, H. Rong, H. Su, L. Sun, S. Wang, Y. Wu, Y. Xu, C. Ying, J. Yu, C. Zha, K. Zhang, Y.-H. Huo, C.-Y. Lu, C.-Z. Peng, X. Zhu, and J.-W. Pan, Realization of an error-correcting surface code with superconducting qubits, *Phys. Rev. Lett.* **129**, 030501 (2022).

[51] S. J. Evered, D. Bluvstein, M. Kalinowski, S. Ebadi, T. Manovitz, H. Zhou, S. H. Li, A. A. Geim, T. T. Wang, N. Maskara, H. Levine, G. Semeghini, M. Greiner, V. Vuletić, and M. D. Lukin, High-fidelity parallel entangling gates on a neutral-atom quantum computer, *Nature* **622**, 268–272 (2023).